THE JOURNAL OF BIOLOGICAL CHEMISTRY VOL. 284, NO. 43, pp. 29921–29934, October 23, 2009


# Kinetic Analysis of Amyloid Formation in the Presence of Heparan Sulfate

## *FASTER UNFOLDING AND CHANGE OF PATHWAY**

Received for publication, May 8, 2009, and in revised form, August 19, 2009 Published, JBC Papers in Press, August 21, 2009, DOI 10.1074/jbc.M109.018747

**Neda Motamedi-Shad[‡], Elodie Monsellier[‡1], Silvia Torrassa[§], Annalisa Relini[§¶], and Fabrizio Chiti[‡¶2]**

*From the [‡]Department of Biochemistry, University of Florence, Viale Morgagni 50, 50134 Florence, Italy, the [§]Dipartimento di Fisica, Università di Genova, Via Dodecaneso 33, 16146 Genoa, Italy, and [¶]Consorzio Interuniversitario "Istituto Nazionale Biostrutture e Biosistemi," Viale delle Medaglie d'Oro, 305, 00136 Rome, Italy*

**A number of human diseases are associated with the conversion of proteins from their native state into well defined fibrillar aggregates, depositing in the extracellular space and generally termed amyloid fibrils. Heparan sulfate (HS), a glycosaminoglycan normally present in the extracellular matrix, has been found to be universally associated with amyloid deposits and to promote amyloid fibril formation by all studied protein systems. We have studied the impact of HS on the amyloidogenesis of human muscle acylphosphatase, monitoring the process with an array of techniques, such as normal and stopped-flow far-UV circular dichroism, thioflavin T fluorescence, static and dynamic light scattering, and atomic force microscopy. The results show that HS accelerates the conversion of the studied protein from the native state into the amyloidogenic, yet monomeric, partially folded state. They also indicate that HS does not simply accelerate the conversion of the resulting partially folded state into amyloid species but splits the process into two distinct pathways occurring in parallel: a very fast phase in which HS interacts with a fraction of protein molecules, causing their rapid aggregation into ThT-positive and β-sheet containing oligomers, and a slow phase resulting from the normal aggregation of partially folded molecules that cannot interact with HS. The HS-mediated aggregation pathway is severalfold faster than that observed in the absence of HS. Two aggregation phases are generally observed when proteins aggregate in the presence of HS, underlying the importance of a detailed kinetic analysis to fully understand the effect of this glycosaminoglycan on amyloidogenesis.**

Deposition of proteins in the form of extracellular amyloid fibrils is a consistent mechanism underlying a group of diverse human diseases, including neurodegenerative disorders and non-neuropathic conditions (1). From a pathogenetic standpoint, these disorders differ by type of aggregated protein and by type of organs involved in amyloid deposition. Among the most prominent neurodegenerative conditions are Alzheimer and Creuzfeldt Jakob diseases, which affect the central nervous system via extracellular deposits. Examples of non-neuropathic systemic amyloidosis are light chain amyloidosis and type II diabetes, where deposits are found in joints, skeletal tissue, and several organs (*e.g.* heart and kidney). Each of these disorders can be traced back to the aberrant conversion of one specific protein or peptide from its soluble, native state into amyloid structures (1). Numerous biochemical and genetic studies have established a widely accepted causative link between pathological symptoms and amyloid structure formation and deposition (2).

Amyloid fibrils are often localized in close proximity to basement membranes, a specialized component of the extracellular matrix that is mainly built of collagens and glycosaminoglycans (GAGs),[3] often attached to a protein core to form the proteoglycans (3–5). GAGs are long unbranched polysaccharides that often occur, with the exception of hyaluronic acid existing in a free form, as *O*- or *N*-linked side chains of proteoglycans, where they regulate the activity of several proteins. Since they have been found physically associated with all types of amyloid deposits *in vivo* so far analyzed, they have been attributed fundamental relevance in amyloidogenesis (3, 4). Of the different types of natural GAGs, heparan sulfate (HS) is among the most important cofactors in amyloid deposits. First, it has been established as a universal component of amyloid, since it has been found to be associated with amyloid deposits of different proteins, including the serum amyloid A protein (6), the immunoglobin light chain (7), transthyretin (8), cystatin C (9), the amyloid β peptide (10), the islet amyloid polypeptide (11), and the prion protein (PrP) (12). More importantly, it has been attributed an active role in amyloidogenesis. Its ability to promote fibrillogenesis has been reported for both the 42- and 40-residue forms of the amyloid β peptide (13, 14), mature islet amyloid polypeptide and proislet amyloid polypeptide 1–48 (15), α-synuclein (16), the 173–243 fragment of D187N gelsolin (17), β2-microglobulin (18), and the tau protein (19). HS has also been found to shift the secondary structure of a subtype of serum amyloid A protein from a random coil to a β-sheet, pre-

* This work was supported in part by grants from the Italian Ministero dell'Istruzione, dell'Università e della Ricerca (Projects PRIN 2006058958 and FIRB RBNE03PX83), the European Union (Project EURAMY), and the European Molecular Biology Organization Young Investigator Program (YIP 2005).

[1] Present address: Laboratoire d'Enzymologie et Biochimie Structurales, CNRS, Gif-sur-Yvette, France.

[2] To whom correspondence should be addressed. Tel.: 39-055-4598319; Fax: 39-055-4598905; E-mail: fabrizio.chiti@unifi.it.

[3] The abbreviations used are: GAG, glycosaminoglycan; AFM, atomic force microscopy; DLS, dynamic light scattering; HS, heparan sulfate; mAcP, human muscle acylphosphatase; PrP, prion protein; TFE, trifluoroethanol; ThT, thioflavin T.

sumably aggregated, structure (20, 21) and to convert the prion protein from the $PrP^{C}$ to the $PrP^{SC}$ form (22).

Despite the large body of data supporting the importance of HS in amyloidogenesis, little is known about the precise mechanism by which HS promotes amyloid formation and the effect that this GAG has on the various phases of the aggregation process and on the overall aggregation pathway. In the current work, human muscle acylphosphatase (mAcP) is utilized to study the impact of HS on amyloid aggregation, with particular attention to the various kinetic phases observed in the presence of this GAG. mAcP represents an enzyme unrelated to any human disease but a particularly suitable model for amyloid aggregation studies for a number of reasons. First, it is small in size (98 residues) and lacks disulfide bridges, *trans*-peptidyl-prolyl bonds, non-proteinaceous cofactors, and other complexities (23, 24). Second, it can form in the presence of 25% (v/v) trifluoroethanol (TFE) amyloid-like fibrils with extensive $\beta$-sheet structure and Congo Red birefringence (25). Third, its aggregation process has been studied using a variety of experimental approaches (25–33) and has been shown to be dramatically influenced by heparin, the highly sulfated form of HS (34).

In the presence of 25% (v/v) TFE, mAcP has been shown to unfold rapidly into a denatured state enriched with $\alpha$-helical structure (25). This partially unfolded state assembles to form, on a time scale of 1–2 h, amyloid-like protofibrils that develop very slowly to form, after a period of several days, long amyloid protofilaments that then associate further to form higher order structures (35). Even the early, protofibrillar aggregates that form within 1–2 h have the ability to bind Congo Red and thioflavin T (ThT) and have an extensive $\beta$-sheet structure, as detected with far-UV CD and Fourier transform infrared spectroscopy (25). This indicates that these protofibrillar structures have the essential structural characteristics of amyloid. The unfolding of the native state into a partially unfolded state is required to initiate aggregation, as shown by the need to use denaturing conditions to start aggregation (27, 35), by the finding that mutations destabilizing the native state promote aggregation (26), and by the observation that ligands binding to and stabilizing the native state have the opposite effect (29). Importantly, the TFE-denatured state of mAcP, which is the most commonly used to trigger aggregation of this protein and will also be used here, is not the only aggregation-competent state of mAcP, since other denatured states of mAcP have been shown to be capable of amyloid fibril formation (27).

The present study aims at investigating the mechanism through which HS influences mAcP aggregation into amyloid-like aggregates. We will investigate both the unfolding and aggregation phases of mAcP in the presence of HS and will monitor them using a variety of biophysical methods. We will show that HS accelerates unfolding in addition to promoting aggregation of the resulting TFE-denatured state, thus playing a double-faced role in the context of its proaggregating effect. We will also show that HS is responsible for the appearance of parallel phases in the aggregation process of this protein and that its effect is not limited to a simple acceleration of the overall process. Following these findings, we will emphasize that a full understanding of the newly generated kinetics is essential for a correct interpretation of the effects of HS on amyloid formation.

## EXPERIMENTAL PROCEDURES

*Materials*—HS ($M_r$ 12,000–14,000) was purchased from Sigma (H7640). Stock solutions were prepared by dissolving an entire vial in $H_2O$ and dividing into 1 mg/ml aliquots that were stored at −20 °C. Each aliquot was discarded after use. ThT (T3516) and TFE (T6,300-2) were purchased from Sigma. mAcP was purified as described previously (36). The mAcP variant utilized here features the mutation C21S, which avoids complexity arising from the presence of free thiol groups (37).

*mAcP Aggregation*—In all experiments, aggregation of mAcP was initiated as previously described (38). Briefly, a mixture was prepared containing 36 $\mu$M mAcP, 25% (v/v) TFE, 50 mM acetate buffer, pH 5.5, at 25 °C. Desired amounts of HS were added to the aggregation mixture, either initially or 10 s after the start of aggregation, to yield final HS concentrations between 0 and 10 $\mu$g/ml. In stopped-flow CD experiments, mAcP concentration varied between 9 and 60 $\mu$M. Beforehand, protein solutions were centrifuged at 20,000 × *g* for 2 min, and protein concentrations were determined by UV absorption using an extinction coefficient ($\epsilon_{280}$) of 1.49 ml $mg^{-1}$ $cm^{-1}$.

*Far-UV Circular Dichroism*—Far-UV circular dichroism experiments were carried out using a Jasco J-810 spectropolarimeter (Tokyo, Japan) equipped with a thermostated cell holder attached to a Thermo Haake C25P water bath (Karlsruhe, Germany). Measurements were acquired in the range 200–250 nm using a 1.0-mm path quartz cuvette at a temperature of 25 °C. Each spectrum was recorded as the average of several scans and was blank-subtracted. Plots of mean residue ellipticity at 215 nm ($[\theta]_{215\ nm}$) *versus* time (*t*) were analyzed with a procedure of best fit, using the single exponential function,

$$[\theta]_{215\ nm}(t) = [\theta]_{215\ nm}(\infty) + A_2 \times \exp(-k_{agg}\, t) \qquad \text{(Eq. 1)}$$

where $[\theta]_{215\ nm}(\infty)$ is the $[\theta]_{215\ nm}$ value at the apparent equilibrium, and $A_2$ and $k_{agg}$ are the amplitude and rate constant of the observed exponential change, respectively.

*Stopped-flow Far-UV Circular Dichroism*—For unfolding experiments, a solution containing mAcP was mixed with 4 volumes of another solution containing 31.25% (v/v) TFE, acetate buffer, pH 5.5, and 0–12.5 $\mu$g/ml HS, where appropriate. Final conditions after mixing were 9–60 $\mu$M mAcP, 25% (v/v) TFE, 50 mM acetate buffer, pH 5.5, and 0–10 $\mu$g/ml HS. For refolding experiments, mAcP was first denatured at a concentration of 180 $\mu$M in 6 M urea at 25 °C for 1 h. This solution was then mixed with 4 volumes of acetate buffer, pH 5.5 and 0–12.5 $\mu$g/ml HS, where appropriate. Final conditions after mixing were 36 $\mu$M mAcP, 1.2 M urea, 50 mM acetate buffer, pH 5.5, and 0–10 $\mu$g/ml HS. A stopped-flow device from Bio-logic (Claix, France) was used for mixing and was coupled to the same far-UV circular dichroism equipment described above. Dead time of the experiment is estimated to be 16 ms. Experiments were carried out at 25 °C.

Plots of mean residue ellipticity ($[\theta]$) *versus* time (*t*) were analyzed with a procedure of best fit, using the single exponential function,

$$[\theta](t) = [\theta](\infty) + A_U \times \exp(-k_U t) \quad \text{(Eq. 2)}$$

or the double exponential function,

$$[\theta](t) = [\theta](\infty) + A_U \times \exp(-k_U t) + A_x \times \exp(-k_x t) \quad \text{(Eq. 3)}$$

where $[\theta](\infty)$ is the $[\theta]$ value at the apparent equilibrium; $A_U$ and $k_U$ are the amplitude and rate constant of the observed exponential change, respectively; and $A_x$ and $k_x$ are the amplitude and rate constant of the second exponential change (when present), respectively. $[\theta](\infty)$, $A_U$, $A_x$, $k_U$, and $k_x$ were used as floating parameters in the procedure of best fit.

*ThT Binding Assay*—Aliquots of the mAcP sample undergoing aggregation (60 $\mu$l) were withdrawn at regular time intervals and mixed with 440 $\mu$l of 10 mM phosphate buffer, pH 6.0, containing 25 $\mu$M ThT, 25 °C. The steady-state fluorescence of the resulting samples was measured at 25 °C using a 2 × 10-mm path length cuvette and a PerkinElmer Life Sciences LS-55 fluorimeter equipped with a thermostated cell compartment attached to a Haake F8 water bath (Karlsruhe, Germany). The excitation and emission wavelengths were 440 and 485 nm, respectively. The dead time of the experiment before the first point can be recorded is estimated at 30 s.

Plots of blank-subtracted fluorescence values *versus* time were analyzed with a procedure of best fit, using the following single exponential function.

$$F(t) = F(\infty) - A_2 \times \exp(-k_{agg} \times t) \quad \text{(Eq. 4)}$$

$F(t)$ and $F(\infty)$ are the fluorescence intensities at time $t$ and $\infty$, respectively, $A_2$ is the amplitude of the observed slow phase, and $k_{agg}$ is its apparent rate constant. $F(\infty)$, $A_2$, and $k_{agg}$ were used as floating parameters in the procedure of best fit. The amplitude of the first fast phase ($A_1$) observed in the presence of HS, was calculated using the following,

$$A_1 = F(\infty) - A_2 \quad \text{(Eq. 5)}$$

where $F(\infty)$ and $A_2$ have the same meaning as in Equation 4. In another experiment, the sample undergoing aggregation and containing 7.5 $\mu$g/ml HS was filtered through a Millex-GV filter unit (SLGVR04NL) from Millipore (Bedford, MA) after 1 min of aggregation and then analyzed similarly.

*Static Light Scattering*—The static light scattering intensity of the mAcP sample undergoing aggregation was measured at regular time intervals at 25 °C using a Jasco V-630 spectrophotometer (Tokyo, Japan), equipped with a Thermo Haake C25P water bath (Karlsruhe, Germany) and a low volume 12.5 × 4.5-mm disposable cuvette. The apparent optical absorption at 400 nm was taken as a measure of scattered light. The light scattered at 75 s, after completion of the first phase and before the second phase has occurred to a significant extent, was taken as an approximate measure of the first phase amplitude. The difference of the light scattering signals at 8000 s, after the completion of the second phase, and at 75 s was taken as an approximate measure of the second phase amplitude.

*Dynamic Light Scattering (DLS)*—Size distributions were acquired, at regular time intervals, for the mAcP sample undergoing aggregation and containing 7.5 $\mu$g/ml HS. Size distributions were also acquired for free HS at concentrations of 7.5 and 400 $\mu$g/ml in 50 mM acetate buffer, pH 5.5, for 36 $\mu$M native mAcP in 50 mM acetate buffer, pH 5.5, and for 72 $\mu$M TFE-denatured mAcP in 70% (v/v) TFE, 50 mM acetate buffer, pH 5.5 (all at 25 °C). Size distributions were acquired using a Zetasizer Nano S DLS device from Malvern Instruments (Malvern, Worcestershire, UK). Low volume 12.5 × 4.5-mm disposable cuvettes were used. A Peltier thermostating system maintained the temperature at 25 °C. For each solution, the viscosity was determined using a V90000 falling ball viscosimeter from Fungilab (Barcelona, Spain), and the refractive index was determined using a 2WAJ ABBE bench refractometer from Optika Microscopes (Bergamo, Italy). The buffer and stock protein solutions were centrifuged (20,000 × *g*, 5 min) and filtered with 0.02-$\mu$m Anotop 10 filters (Whatman, Maidstone, UK) before the measurements.

*Atomic Force Microscopy (AFM)*—Aliquots of the mAcP sample undergoing aggregation were extracted at fixed times and diluted 100 times with Milli-Q water; in each case, a 10-$\mu$l aliquot of the diluted sample was immediately deposited on freshly cleaved mica and dried under a vacuum. AFM measurements were performed with a Dimension 3100 scanning probe microscope (Digital Instruments Veeco, Santa Barbara, CA) equipped with a G scanning head (maximum scan size 100 $\mu$M) and controlled by a Nanoscope IIIa controller. AFM images were acquired in tapping mode in air; single beam uncoated silicon cantilevers (type OMCL-AC160TS, Olympus, Japan) were used. The drive frequency was around 300 kHz; the scan rate was between 0.5 and 2.0 Hz. Images were collected with 512 data points/line.

Aggregate sizes were measured from the height in cross section of the topographic AFM images; the measured heights were multiplied by a factor of 2.2, to correct for dehydration effects. The correction factor was evaluated comparing the heights of a globular protein (native HypF-N) under liquid and in air after drying under vacuum.

## RESULTS

*HS Accelerates the Initial Conformational Change of Native mAcP*—Aggregation of mAcP was induced by incubating the protein, at a concentration of 36 $\mu$M, in 25% (v/v) TFE, 50 mM acetate buffer, pH 5.5, at 25 °C. Under these conditions, the protein rapidly converts from its native structure into a non-native TFE-denatured state enriched with $\alpha$-helical structure, which subsequently aggregates (35, 39). In order to monitor this early event, a stopped-flow device coupled to a CD detection system was used. In this experiment, a solution containing the native protein in the absence of TFE was mixed with another solution containing TFE. The final conditions after mixing are those reported above (36 $\mu$M mAcP, 25% (v/v) TFE, 50 mM acetate buffer, pH 5.5, 25 °C). The mean residue ellipticity at 216 nm ($[\theta]_{216}$) undergoes a rapid exponential decrease toward a more negative value (Fig. 1*A*). Such a decrease is expected, since the TFE-denatured state possesses a more negative value of mean residue ellipticity at this wavelength than the native state (39). The rate constant value of such an exponential decrease ($k_U$), obtained using a

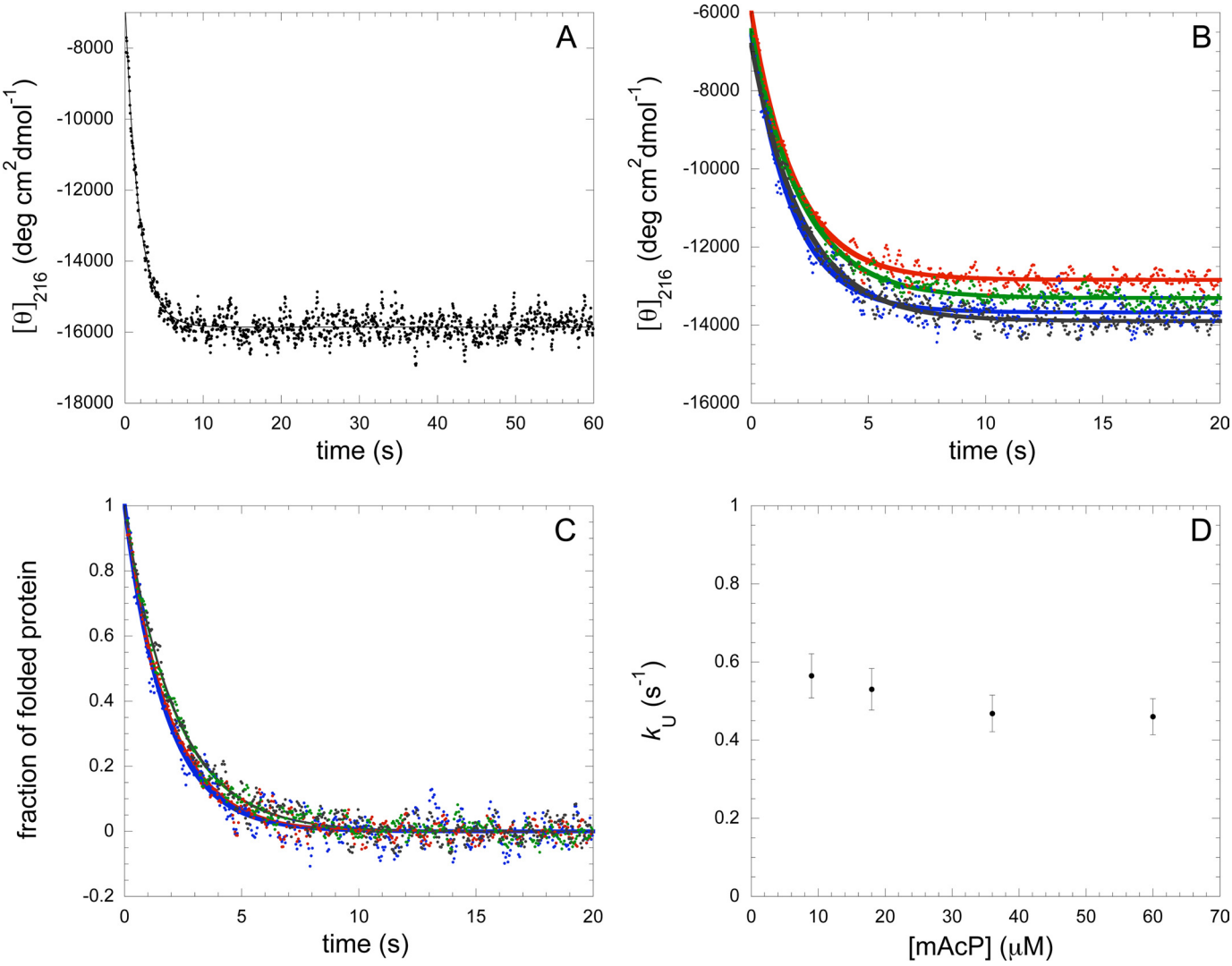


FIGURE 1. *A*, conformational change occurring for mAcP under aggregating conditions within the first 60 s, monitored by stopped-flow CD at 216 nm. mAcP was incubated at a concentration of 36 $\mu$M in 25% TFE (v/v), 50 mM acetate buffer, pH 5.5, at 25 °C. *B* and *C*, the same experiment as in *A*, carried out at concentrations of mAcP of 9 $\mu$M (*blue*), 18 $\mu$M (*red*), 36 $\mu$M (*green*), and 60 $\mu$M (*black*). *C*, the kinetic traces reported in *B* were normalized as fraction of folded protein. In *A–C*, the *solid lines* through the data points result from a procedure of best fit using a single exponential function (Equation 2). *D*, lack of dependence of the rate constant ($k_U$) for the observed exponential decrease of $[\theta]_{216}$ on mAcP concentration. *Error bars*, 10% of reported values, represent variations that are typically observed.

procedure of best fit and a single exponential function (Equation 2), was estimated to be 0.57 ± 0.01 $s^{-1}$.

To assess whether the observed exponential change of $[\theta]_{216}$ is attributable to an unfolding event (*i.e.* to a conformational change involving monomeric mAcP) or rather to an early aggregation event, the experiment was repeated at different protein concentrations, ranging from 9 to 60 $\mu$M. The resulting kinetic traces, normalized to $[\theta]_{216}$, are superimposable and exhibit similar values of $k_U$ as well as similar values of initial and final $[\theta]_{216}$ (Fig. 1, *B–D*). This indicates that the observed change of $[\theta]_{216}$ can be attributed to a conformational change of the monomer rather than to an early event of aggregation, which by contrast would be expected to have a marked dependence on protein concentration. Moreover, the $k_U$ value determined from such an exponential decrease is similar to that of mAcP unfolding previously determined under similar conditions (29) and much more rapid than that of aggregation in these conditions (35).

The experiment was then repeated, under identical conditions, in the presence of various concentrations of HS ranging from 0 to 10 $\mu$g/ml (Fig. 2*A*). The observed exponential decrease of $[\theta]_{216}$ becomes more rapid as the concentration of HS increases. The $k_U$ value obtained from such an analysis features a marked dependence on HS concentration (Fig. 2*B*). The addition of HS causes an increase of the $k_U$ value of ~2-fold. A marked dependence was found particularly between 0 and 5 $\mu$g/ml with no further changes occurring upon further increase of HS concentration (Fig. 2*B*).

We also monitored the effect of HS on the refolding rate of mAcP. This was achieved by diluting the protein denatured in 6 M urea into a buffer containing no denaturant. Final conditions after mixing were 36 $\mu$M mAcP, 1.2 M urea, 50 mM acetate buffer, pH 5.5, 25 °C. In order to perform these experiments, it was necessary to apply solution conditions different from those used to study unfolding, since in 25% (v/v) TFE, the native protein is unstable, and refolding cannot be monitored. The choice

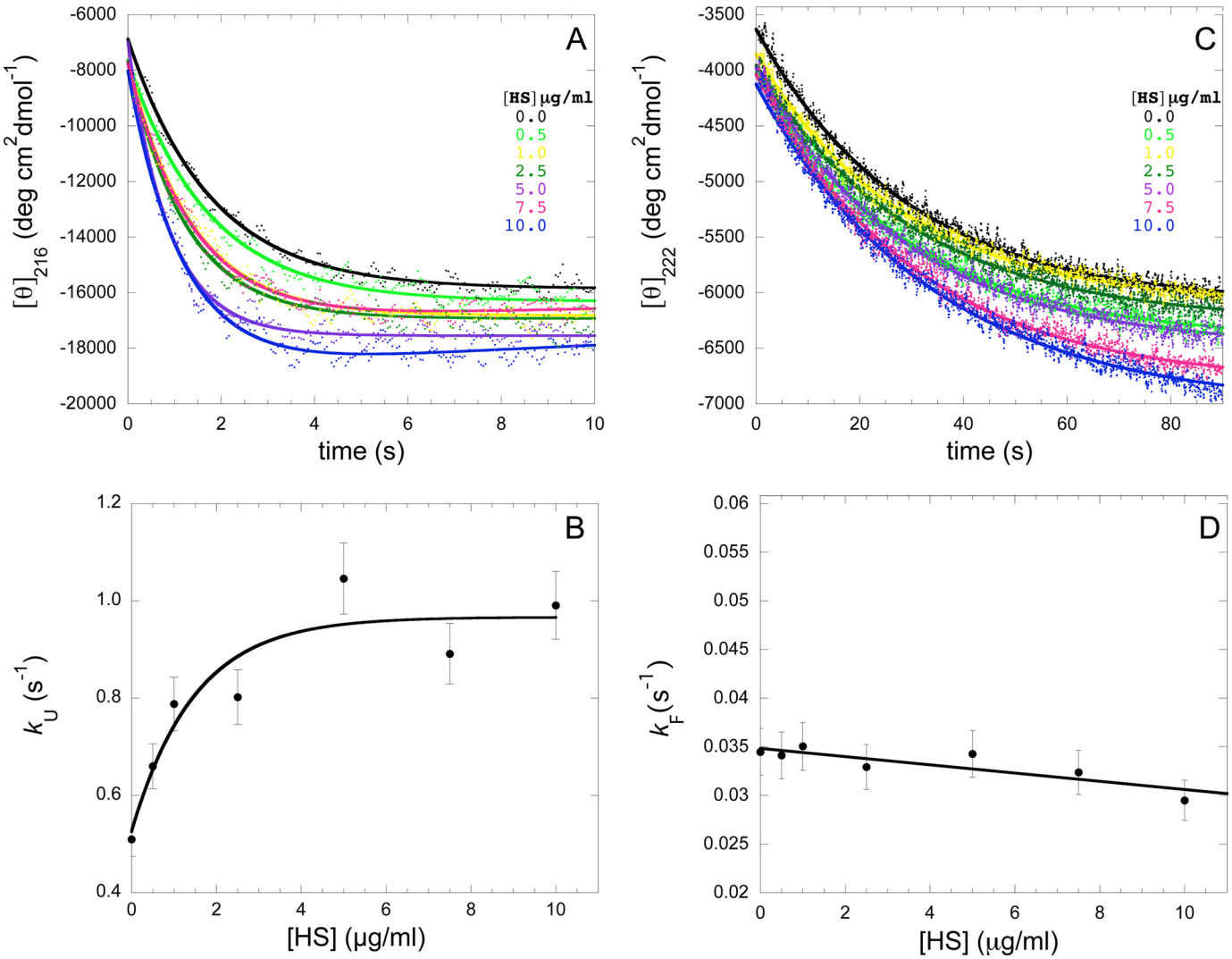


FIGURE 2. *A*, conformational change occurring for mAcP under aggregating conditions within the first 10 s at varying concentrations of HS, monitored by stopped-flow CD. mAcP was incubated at a concentration of 36 $\mu$M in 25% TFE (v/v), 50 mM acetate buffer, pH 5.5, at 25 °C with 0–10 $\mu$g/ml HS. *B*, dependence of $k_U$ on HS concentration. The *solid line* through the data points represents the observed trend. *C*, refolding of mAcP after unfolding in 6 M urea at varying concentrations of HS, monitored by stopped-flow CD. Final conditions were 36 $\mu$M mAcP, 1.2 M urea, 50 mM acetate buffer, pH 5.5, at 25 °C with 0–10 $\mu$g/ml HS. *D*, minor dependence of $k_F$ on HS concentration. The *solid line* through the data points represents the observed trend. In *B* and *D*, *error bars* represent S.E. of 7%, which are routinely observed during such experiments.

of the urea-denatured state as the initial state, as opposed to the TFE-denatured state, is not an issue, since refolding is well known to be independent of the initial unfolding conditions. Refolding of the protein from the urea-denatured state involves a decrease of the $[\theta]_{222}$ value (Fig. 2*C*). We have also observed a decrease of the $[\theta]_{216}$ value during the conformational change from the native to the aggregation-prone state in 25% (v/v) TFE (Fig. 2*A*). This arises from the fact that the $[\theta]_{222}$ value decreases progressively upon going from the urea-unfolded ($[\theta]_{222} \sim -3500 \pm 1000$ degrees cm$^2$ dmol$^{-1}$) to the native state ($[\theta]_{222} \sim -6500 \pm 1000$ degrees cm$^2$ dmol$^{-1}$) and then to the TFE-denatured state ($[\theta]_{222} \sim -15{,}000 \pm 1000$ degrees cm$^2$ dmol$^{-1}$).

The refolding experiment was repeated, under identical conditions, in the presence of various concentrations of HS ranging from 0 to 10 $\mu$g/ml (Fig. 2*C*). The rate constant value of the observed exponential decrease ($k_F$), obtained using again a procedure of best fit and a single exponential function (Equation 2), was found to undergo a very small decrease, if any, as the concentration of HS increases (Fig. 2*D*). Overall, HS increases the conversion rate of the native state into the TFE-denatured state but does not affect significantly the folding rate, resulting in a global thermodynamic destabilization of the native state in addition to a kinetic acceleration of its conversion into the aggregation-prone state.

*HS Induces Rapid Accumulation of Species with β-Sheet Structure*—In the absence of HS, the relatively fast transition of mAcP from its native state into a denatured state with extensive $\alpha$-helical content is followed by a slow phase in which the resulting TFE-denatured mAcP self-assembles to form aggregates with a considerable amount of $\beta$-sheet structure (35). In order to assess the impact of HS on this slow transition phase, the conversion was first monitored using far-UV CD. In the absence of HS, spectra acquired at regular time intervals indicate a slow transition from an $\alpha$-helical spectrum, acquired after 4 min, to a highly $\beta$-sheet

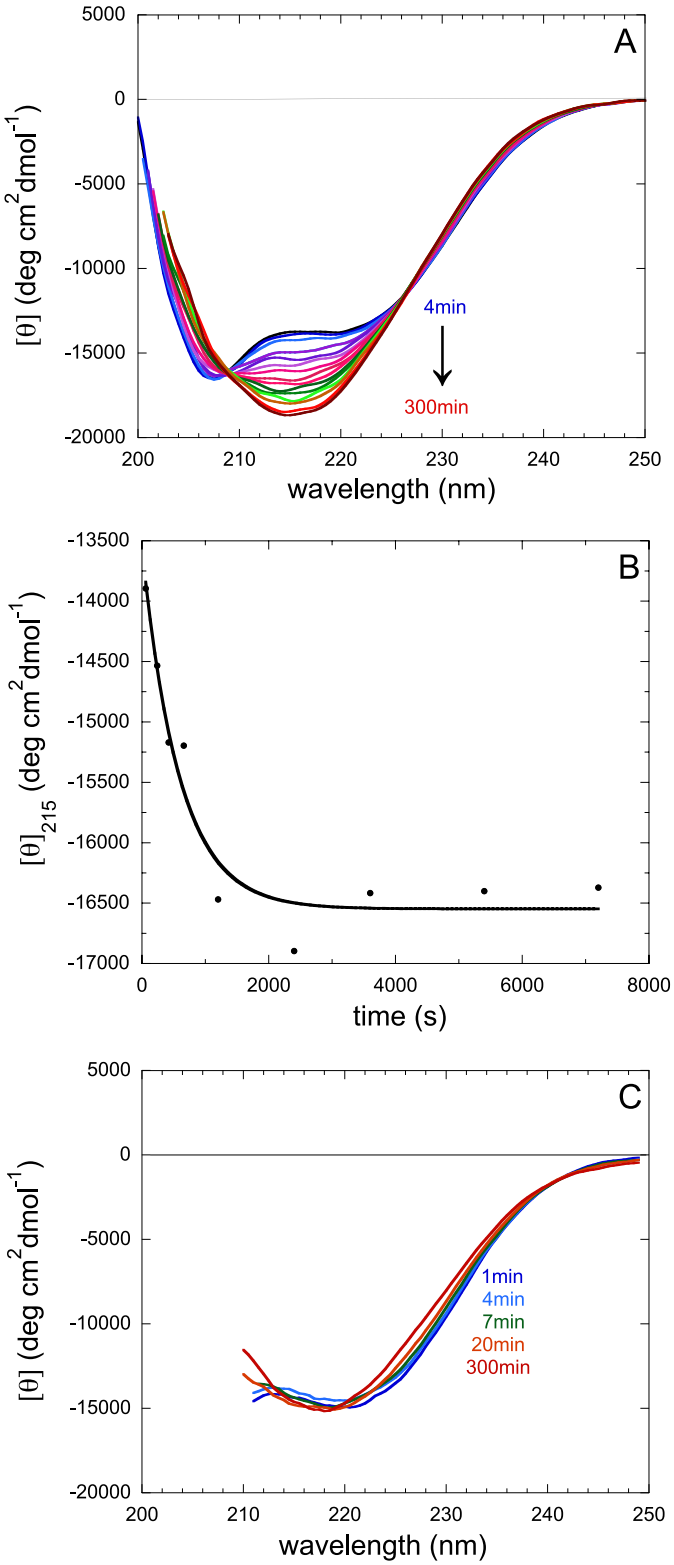


FIGURE 3. *A*, far-UV CD spectra of mAcP acquired during the aggregation process in the absence of HS. mAcP was incubated as described in the legend to Fig. 1*A*. The first and the last spectra reported here were acquired after 4 min and 5 h, respectively. *B*, time course of the $[\theta]_{215}$ value during aggregation of mAcP in the absence of HS. mAcP was incubated as described in the legend to Fig. 1*A*, and the $[\theta]_{215}$ value was recorded at regular time intervals. The *solid line* through the data points results from a procedure of best fit using a single exponential function (Equation 1). *C*, far-UV CD spectra of mAcP acquired during the aggregation process in the presence of HS. mAcP was incubated under the same conditions with 7.5 $\mu$g/ml HS. The spectra reported here were acquired after 1 min (*blue*), 4 min (*pale blue*), 7 min (*green*), 20 min (*orange*), and 5 h (*red*).

spectrum after 5 h (Fig. 3*A*). The experiment was also carried out, still in the absence of HS, under conditions identical to those used for stopped-flow CD and recording the $[\Theta]_{215}$ value at regular time intervals during the aggregation process (Fig. 3*B*). The $[\Theta]_{215}$ value was found to decrease until a constant value was observed after ~1 h. The obtained time course could be fitted satisfactorily to a single exponential function (Equation 1) yielding a rate constant of $1.70 \pm 0.42 \times 10^{-3}$ s$^{-1}$. Protein aggregation is clearly a multimolecular process with kinetics more complicated than first-order and approaching, in the most simple case, pseudo-first-order kinetics. The kinetic data presented here and later on are analyzed with single exponential kinetics as an approximation, to yield a gross measure of the aggregation rate.

The experiment was then repeated, under identical conditions, in the presence of 7.5 $\mu$g/ml HS (Fig. 3*C*). The first far-UV CD spectrum acquired after 1 min is predominantly $\alpha$-helical but differs clearly from the initial spectra acquired in the absence of HS and rather resembles those recorded at intermediate time points during the aggregation transition in the absence of HS, when $\beta$-sheet structure is partially present. This picture is complemented by spectra acquired after 4, 7, and 20 min, which appear to result from increasingly enhanced $\beta$-sheet structure formation (Fig. 3*C*). The last spectrum acquired after 5 h indicates extensive $\beta$-sheet structure and resembles that acquired in the absence of HS at this advanced time point. Similarly to the experiment performed in the absence of HS, we also attempted to follow the time course of aggregation in the presence of 7.5 $\mu$g/ml HS by monitoring the $[\theta]_{215}$ value. However, the $[\theta]_{215}$ value does not show a detectable difference in the initial and final spectra (Fig. 3*C*), making the kinetic trace of $[\theta]_{215}$ as a function of time dominated by noise in this case.

*HS Promotes the Appearance of a New Rapid Phase of Aggregation*—In the next set of experiments, the time course of aggregation in the presence of various concentrations of HS, ranging from 0 to 10 $\mu$g/ml, was monitored performing ThT binding assays at regular time intervals. Plotting single measurements of ThT fluorescence as a function of time allowed us to follow the time courses of aggregation in the presence and absence of various concentrations of HS (Fig. 4*A*). In the absence of HS, a single phase is observed, and the resulting trace could be fitted to a single exponential function (Equation 4), yielding a value of $1.11 \pm 0.2 \times 10^{-3}$ s$^{-1}$. This value is similar, within experimental error, to the value obtained with far-UV CD ($1.70 \pm 0.42 \times 10^{-3}$ s$^{-1}$), indicating that the transitions monitored with the two spectroscopic probes result from essentially the same aggregation phase.

In the presence of HS, the obtained time courses are dominated by two kinetic phases (Fig. 4*A*). In a first phase, occurring on a time scale of a few seconds and going to completion before the first ThT fluorescence measurement can be carried out, the ThT fluorescence increases significantly, to an

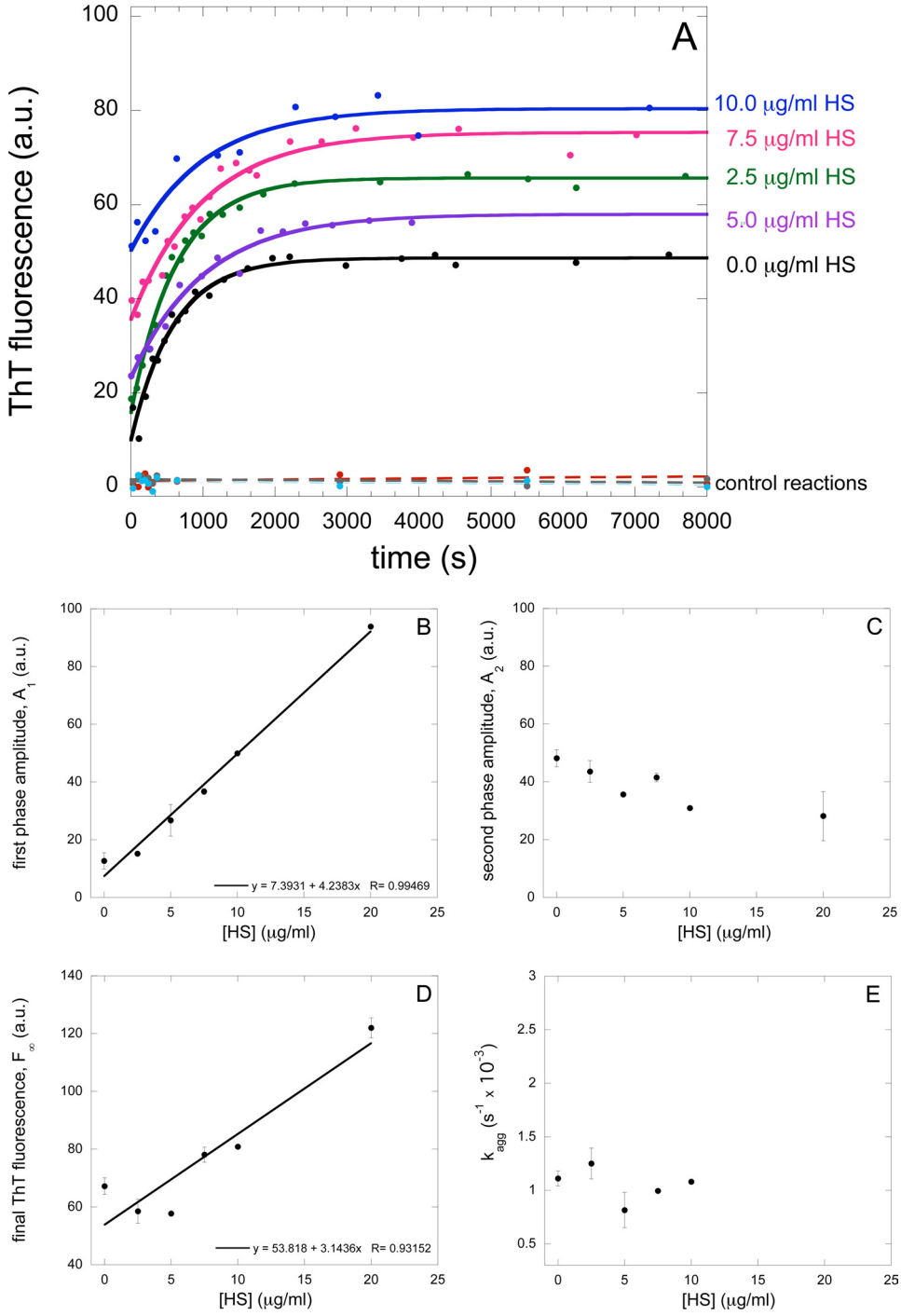


FIGURE 4. *A*, time course of the ThT fluorescence during mAcP aggregation in the absence and presence of various concentrations of HS. mAcP was incubated as described in the legend to Fig. 1*A* with 0–10 μg/ml HS. For each HS concentration tested, aliquots of the aggregating mixture were taken at regular time intervals and used for the ThT assay. As control reactions, samples containing denatured mAcP in 8 M urea (*gray*), native protein in acetate buffer (*red*), and HS in acetate buffer without mAcP (*pale blue*) were also monitored. *B* and *D*, dependence of the first phase amplitude and the final ThT fluorescence on HS concentration. *C* and *E*, lack of dependence of the amplitude and rate constant of the second kinetic phase on HS concentration. *Solid lines* through the data points result from a procedure of best fit using a single exponential (Equation 4) function (*A*) or a linear function (*B* and *D*). *Error bars*, S.E. values resulting from at least three independent experiments. *a.u.*, arbitrary units.

extent that is dependent on HS concentration (Fig. 4*A*). This fast phase is followed by a slow phase occurring on a time scale comparable with that found in the absence of HS. This indicates that HS induces the appearance of a new rapid phase occurring within the dead time of our experiment and causing a rapid increase of ThT fluorescence. A linear dependence between HS concentration and the amplitude of the first fast phase, determined as described under "Experimental Procedures," was observed (Fig. 4*B*). By contrast, the amplitude of the second slow phase is independent of HS concentration or exhibits just a slight negative dependence (Fig. 4*C*). The final ThT fluorescence was also found to increase linearly with HS concentration, mainly as a consequence of the appearance of the fast phase in the presence of this GAG (Fig. 4*D*).

The time course of the second slow phase does not appear to be affected by the presence of HS, since the obtained rate constant values ($k_{agg}$) do not correlate with the concentrations of HS that were used (Fig. 4*E*). As control experiments, the ThT fluorescence was also measured in the presence of 7.5 μg/ml HS in buffer without mAcP, native mAcP with no HS, and mAcP denatured in 8 M urea without HS (Fig. 4*A*). In all cases, the ThT fluorescence remained low, indicating that the initial increase of ThT fluorescence upon the addition of HS is due to real protein aggregation, since neither HS nor monomeric mAcP, independently of its conformational state, has the ability to increase the ThT fluorescence.

The aggregation process of mAcP in the presence of various concentrations of HS, ranging from 0 to 10 μg/ml, was also monitored using light scattering (Fig. 5*A*). In the presence of HS, two phases were again observed: an initial rapid increase, occurring within the dead time of the experiment, followed by a slower increase. This latter increase occurred on a time scale comparable with that observed with ThT fluorescence and apparently independently of HS concentration. Unfortunately, light scattering continued to increase after this initial phase, probably as a result of further association or reorganization of the aggregates, preventing an accurate analysis with a sin-

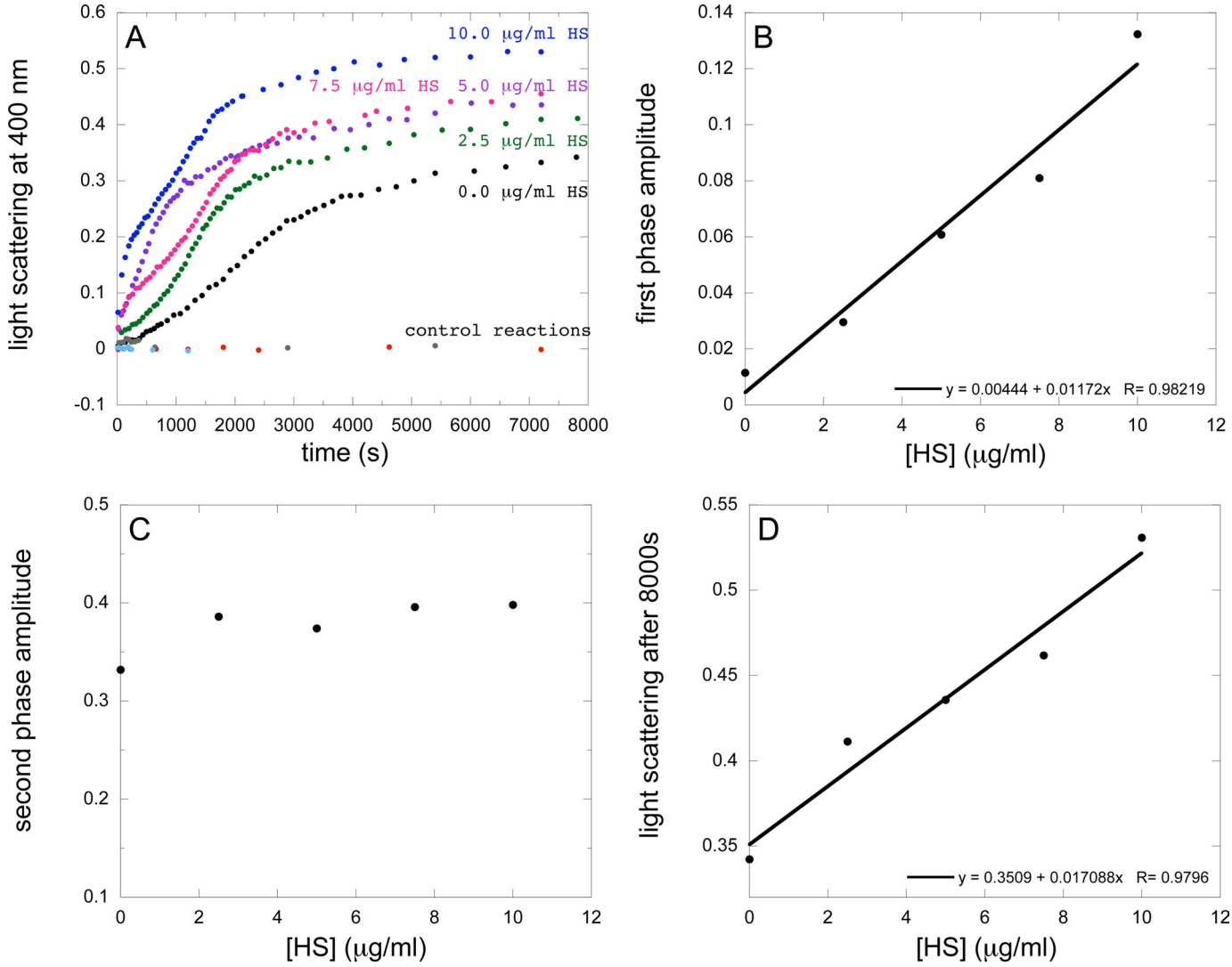


FIGURE 5. *A*, mAcP aggregation in the absence and presence of various concentrations of HS followed by monitoring light scattering at 400 nm. mAcP was incubated as described in the legend to Fig. 1*A* with 0–10 μg/ml HS. As control reactions, samples containing denatured protein in 8 M urea (*gray*), native protein in acetate buffer (*red*), and HS in acetate buffer without protein (*pale blue*) were also monitored. *B*, dependence of the first phase amplitude on HS concentration. *C*, lack of dependence of the second phase amplitude on HS concentration. *D*, dependence of final light scattering measured at 8000 s on HS concentration. In *B* and *D*, the *solid lines* through the data points result from a procedure of best fit using a linear function.

gle exponential function and, as a consequence, of an accurate determination of $k_{agg}$ values. The amplitudes of the first and second phases, determined as described under "Experimental Procedures," are plotted as a function of HS concentration in Fig. 5, *B* and *C*. Similarly to the ThT binding analysis, the first phase amplitude increases linearly with HS concentration (Fig. 5*B*), whereas the second phase amplitude does not have a remarkable dependence on HS concentration (Fig. 5*C*). The light scattering signal recorded after the second phase was also found to increase with HS concentration (Fig. 5*D*).

As control reactions, the time dependences of light scattering for native mAcP in buffer, denatured mAcP in 8 M urea, and 7.5 μg/ml HS in buffer, without mAcP, were also monitored (Fig. 5*A*). All of the control reactions resulted in scattering signals around zero, indicating that the initial increase of light scattering signal upon the addition of HS is due to real protein aggregation, since neither HS nor monomeric mAcP, independently of its conformational state, scatter light.

*The Two Aggregation Phases Are Parallel Rather Than Sequential Events*—In both ThT binding assays and light scattering experiments, a very rapid formation of initial aggregates was observed when HS was present (Figs. 4*A* and 5*A*). In principle, the two kinetic phases observed in the presence of HS can be two steps of a sequential mechanism, where the TFE-denatured state converts into aggregates (first phase), which consequently convert or assemble further to form other aggregates (second phase). Alternatively, the two phases can be two events occurring in parallel, both consisting of the assembly of the TFE-denatured state into aggregates and where only the first fast phase is dependent on HS. The data obtained so far account for the second mechanism rather than the first (see "Discussion"), but to obtain a more strong indication that the phases reflect parallel events, a specific test was performed.

mAcP aggregation was initiated under identical conditions, in the presence of 7.5 μg/ml HS, but after 1 min the sample was filtered. The first phase is complete after 1 min, whereas the second phase has just started (Figs. 4*A* and 5*A*). The resulting filtrate was subjected, at regular time intervals, to ThT binding assays as described before. The comparison of the two ThT fluorescence time courses obtained with and without filtration in the presence of 7.5 μg/ml HS is shown in Fig. 6*A*. In the filtered sample, the initial ThT fluorescence value obtained immediately after filtration was found to be similar to that obtained in the unfiltered sample in the absence of HS and remarkably lower than that obtained in the unfiltered sample containing HS (Fig. 6*A*). In the filtered sample, the ThT fluorescence was then found to increase in a time frame similar to that reported for the unfiltered sample (Fig. 6*A*). The amplitude of the change is lower in the filtered sample, as a consequence of the fact that the effective protein concentration is lowered by removing initial aggregates and partly also soluble protein through filtration (data not shown). In summary, the filtration removes the fast phase but preserves the slow phase, thus reverting the behavior of the sample to that observed in the absence of HS.

In another experiment, HS was added, to a final concentration of 7.5 μg/ml, 10 s after the start of the aggregation process rather than concomitantly. Interestingly, the kinetic trace monitored with ThT fluorescence is superimposable to that obtained in the absence of HS and different from that acquired when a similar concentration of HS is present at the start of the reaction (Fig. 6*B*). In fact, no first phase is present when HS is added with a delay of 10 s. This indicates that the interaction between mAcP and HS occurs early in the process, before the protein is denatured to form the aggregation-prone state. Hence, the fast phase of aggregation monitored with ThT and light scattering involves the aggregation process of a fraction of initially native protein molecules that bind to HS, unfold after binding, and immediately aggregate on the HS surface.

*Aggregates and the TFE-denatured State Coexist after the First Phase*—The aggregation process of mAcP in the presence of 7.5 μg/ml HS was also monitored using DLS. First, the apparent hydrodynamic diameters of native mAcP in acetate buffer, TFE-denatured mAcP in 70% TFE, and of HS in acetate buffer with no protein, at concentrations of 7.5 and 400 μg/ml, were measured (Fig. 7*A*). Native mAcP appears to have a hydrodynamic diameter of 3.6 ± 0.1 nm, a value consistent with the NMR structure of this protein (23). The TFE-denatured state of mAcP in 70% (v/v) TFE, a concentration of TFE where aggregation does not occur to any detectable extent (26), is 7.5 ± 0.4 nm. Finally, the apparent hydrodynamic diameter of HS was found to be 10.1 ± 2.4 nm, a value consistent for a HS molecule of this size (12–14 kDa) and the typical rigidity provided by the negatively charged moieties. The sample containing 7.5 μg/ml HS did not scatter the light to any detectable extent with our apparatus (Fig. 7*A*), indicating that any signal obtained in aggregation experiments performed in the presence of 7.5 μg/ml does not arise from free HS in solution.

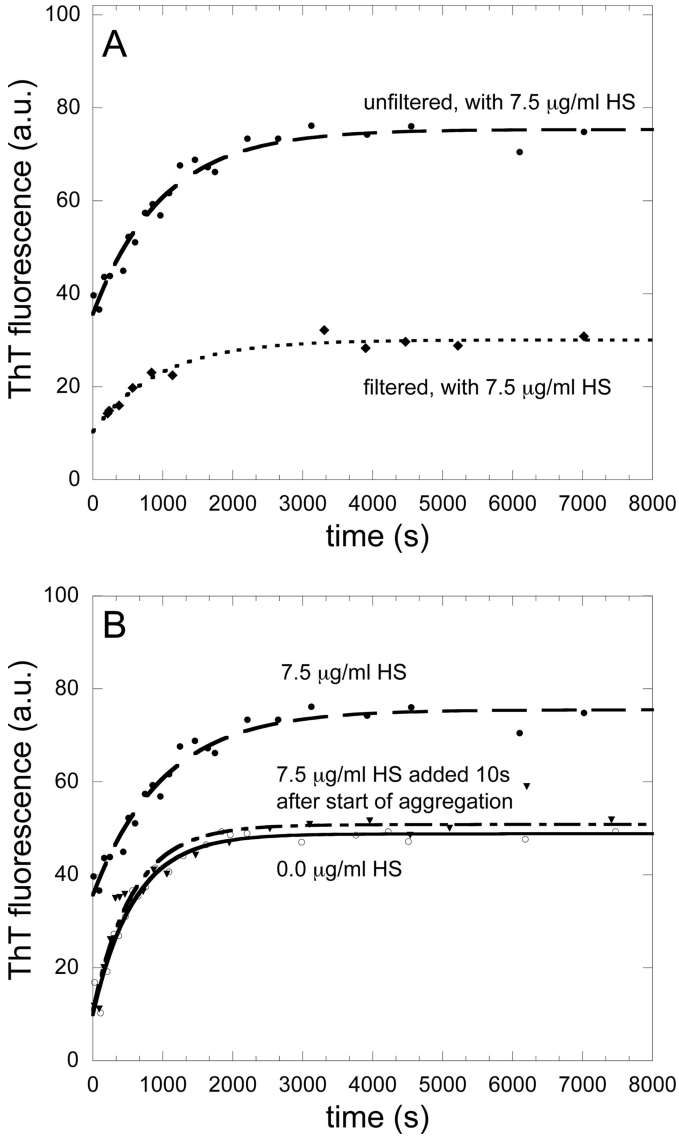


FIGURE 6. *A*, time course of the ThT fluorescence during mAcP aggregation in the presence of HS after initial aggregates were removed by filtration. mAcP was incubated as described in the legend to Fig. 1*A* with 7.5 μg/ml HS, and the sample was filtered after 1 min from the start of aggregation (*dotted line*). The time course obtained for the unfiltered sample with 7.5 μg/ml HS is also shown for comparison (*dashed line*). *B*, time course of the ThT fluorescence during mAcP aggregation when HS is added 10 s after the start of the aggregation process. mAcP was incubated as described in the legend to Fig. 1*A*, and 7.5 μg/ml HS was added 10 s after the start of the reaction (*dashed and dotted line*). The time courses obtained in the absence of HS (*solid line*) and when 7.5 μg/ml HS was initially present (*dashed line*) are shown for comparison. *a.u.*, arbitrary units.

When mAcP was incubated under our standard aggregating conditions in the presence of 7.5 μg/ml HS, the size distribution acquired after 40 s revealed two distinct populations with apparent hydrodynamic diameters of ~6.5 nm, which is very similar to the hydrodynamic diameter obtained for the monomeric TFE-denatured state of mAcP, and 78.8 nm, arising from mAcP aggregates. Since the light scattering intensity scales with the square of the mass of the particles in solution, the presence of a peak at 6.5 nm, albeit small, indicates that the TFE-denatured state is by far the predominant species at this time, coexisting with a fair amount of protein aggregates. The time of this

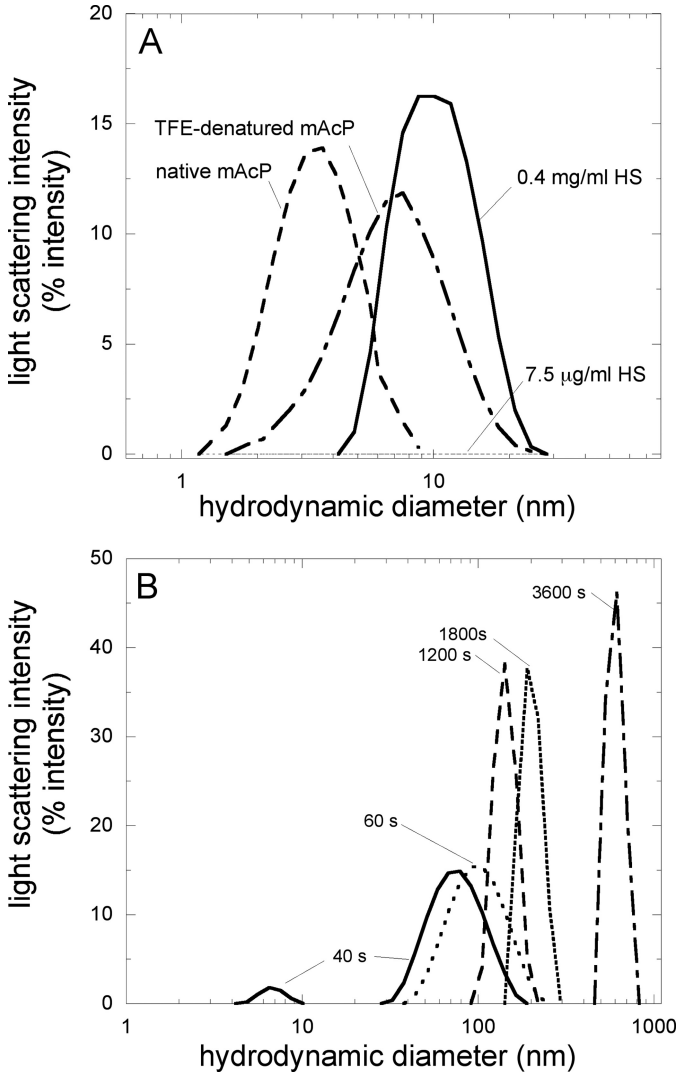


FIGURE 7. **Size distribution of mAcP during the aggregation process in the presence of 7.5 μg/ml HS determined using DLS.** mAcP was incubated as described in the legend to Fig. 1*A* with 7.5 μg/ml HS. *A*, hydrodynamic diameters of 7.5 μg/ml HS (*dotted line*), 400 μg/ml HS (*solid line*), mAcP denatured in 70% (v/v) TFE (*dashed and dotted line*), and native mAcP (*dashed line*) were also acquired, all in 50 mM acetate buffer, pH 5.5, 25 °C. *B*, size distributions of mAcP in 50 mM acetate buffer, pH 5,5, with 7.5 μg/ml HS acquired after 40 s (*solid line*), 1 min (*dotted line*), 20 min (*dashed line*), 30 min (*pixilated line*), and 1 h (*dashed and dotted line*).

measurement corresponds to a stage where the first phase is completed and the slow phase has not occurred to any significant extent (Figs. 4*A* and 5*A*). The co-existence, in the size distribution obtained with DLS, of peaks at ~80 and 6.5 nm confirms the presence of aggregates at this stage, co-existing with a large quantity of monomeric protein that has not yet undergone aggregation.

At later times, a signal arising from monomeric, TFE-denatured mAcP was no longer detected with DLS, mainly because the growing population and growing size of the aggregates obscured the detection of this species. The aggregates detected with DLS increased in size, also obscuring the detection of smaller aggregated species that possibly remained in the sample (Fig. 7*B*).

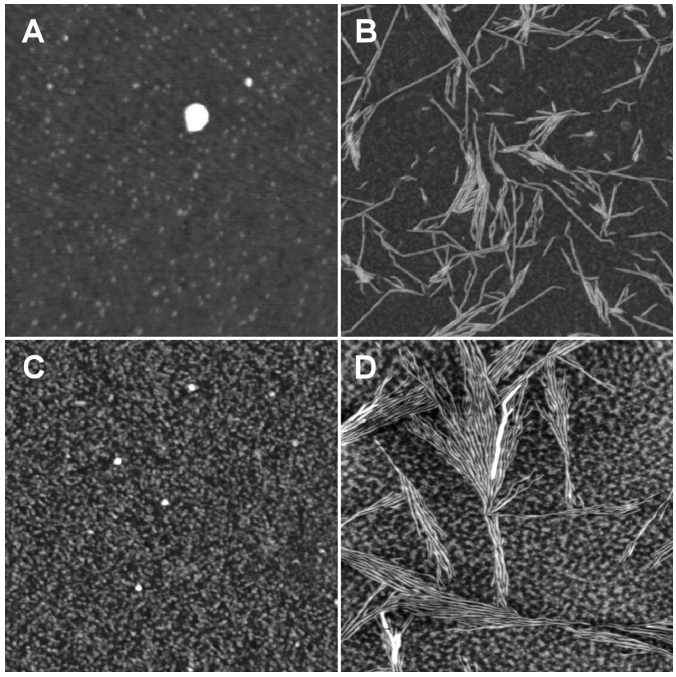


FIGURE 8. **Tapping mode AFM images (height data) of mAcP aggregation in 25% (v/v) TFE, 50 mM acetate buffer, pH 5.5, 25 °C in the absence and presence of HS.** Protein concentration was 0.4 mg/ml. *A*, at the start of the aggregation process, in the absence of HS. *B*, after 1 h aggregation, in the absence of HS. *C*, at the start of the aggregation process, in the presence of 7.5 μg/ml HS. *D*, after 1 h aggregation, in the presence of 7.5 μg/ml HS. Scan size is 1 μm (*A* and *C*) or 2 μm (*B* and *D*). *Z* range is 5.0 nm (*A*), 10.0 nm (*B*), 3.0 nm (*C*), or 8.0 nm (*D*).

*The Two Phases of Aggregation Lead to the Formation of Oligomers and Protofibrils, Respectively*—Tapping-mode AFM was also used to analyze the morphology of the aggregates formed in the presence and absence of HS. In the absence of HS, after a few seconds of incubating mAcP in TFE, no significant amount of aggregates was seen in the AFM images (Fig. 8*A*). By contrast, protofibrils with mean height of 6.2 ± 0.1 nm were present after 1 h of incubation (Fig. 8*B*). Isolated globular structures with mean height of 2.1 ± 0.1 nm were also observed (data not shown). When the analysis was repeated in the presence of 7.5 μg/ml HS, a large number of oligomeric, non-fibrillar species were present immediately after the start of the aggregation reaction (Fig. 8*C*). After 1 h of incubation under the same conditions, the AFM images showed the presence of both oligomers and protofibrils with mean heights of 3.9 ± 0.1 nm and 6.9 ± 0.1 nm, respectively (Fig. 8*D*). These images suggest that in the new rapid phase of aggregation that is induced by the presence of HS, small oligomers are formed, whereas a second slow phase of aggregation, which occurs independently of HS in the sample, leads to the formation of protofibrillar species. At the end of the second slow phase, mAcP oligomers that have interacted with HS but are not yet transformed into fibrils coexist with protofibrils that were formed, which suggests again a parallel nature of the two aggregation phases.

## DISCUSSION

HS has been found to be universally associated with all the amyloid deposits analyzed so far (6–12) and has been found to

promote amyloid fibril formation *in vitro* by all studied protein systems (13–22). In particular, it is generally reported that HS causes an increase of the rate by which fibrils are formed (13–17, 22) and of the final ThT fluorescence (14–17). The study presented here on mAcP has revealed two important and previously unexplored effects of HS, *i.e.* the ability of this GAG (i) to decrease the thermodynamic stability of the folded state and accelerate its conversion into an aggregation-competent partially folded state and (ii) to cause the appearance of a novel kinetic phase in which ordered aggregates with an ability to bind ThT and β-sheet structure form very rapidly. The following two paragraphs will discuss these two findings separately.

*Acceleration of the Initial Conformational Change of Native mAcP by HS*—Although HS was not found to have a significant effect on the refolding rate of mAcP, the conversion of the initial native state into the TFE-denatured state has been found to be accelerated 2-fold under the conditions of mAcP and HS concentrations studied here. It was previously shown that compounds containing phosphate and sulfate groups are able to bind native mAcP via interactions with the active site of this enzyme, with dissociation constants on the order of 0.1 mM under conditions of pH, TFE concentration, and temperature similar to those studied here (29). The addition of such molecules has been found to decelerate, rather than accelerate, the conversion from the native to the TFE-denatured state as binding stabilizes the native state of mAcP (29). The conditions employed here are, however, different. The lowest HS concentration shown here to cause a significant acceleration of this conformational transition is 5 μg/ml, corresponding to an effective concentration of sulfate moieties of ~17 μM, 1 order of magnitude lower than the dissociation constant of sulfate- and phosphate-containing compounds for native mAcP. Consequently, the expected deceleration of the conversion into the TFE-denatured state, mediated by a direct binding to the native active site, is negligible in our experiments. In addition, the sulfate moieties present on HS may have a lower accessibility to the mAcP active site than free sulfate-containing small molecules. In the experimental study presented here, the effect of the sulfate moieties on the rate of conversion of the native state into the TFE-denatured state is of a different nature, specific for HS and resulting in acceleration rather than deceleration.

The HS-mediated acceleration of the initial conformational change involving the native state and the resulting decrease of the thermodynamic stability of such a state can be important in the amyloidogenesis of proteins that are initially folded and that are associated with clinical amyloidosis, such as transthyretin, β2-microglobulin, immunoglobulin light chains, lysozyme, and others. For all of these proteins, mild denaturing conditions that destabilize the native state, such as low pH, high temperature, or high pressure, have been found to promote aggregation (40–43). In addition, mutations destabilizing the native states of these proteins are all promoting fibrillogenesis (40, 44–46). These two lines of evidence indicate that initially folded proteins need to unfold, at least partially, to initiate aggregation. It has been recently emphasized that amyloid formation does not necessarily require a process of unfolding across the major free energy barrier for unfolding but rather local structural perturbations from the native state (47). It is clear, however, that mutational, chemical, and physical agents that destabilize the native state of a protein favor both unfolding and structural fluctuations. In conclusion, given the importance of a structural transition involving the native state, either global or local, the kinetic and thermodynamic effect of HS on this transition emphasizes one more proaggregating effect of HS, which adds to the well established proaggregating effect occurring during the subsequent aggregation steps.

*Appearance of a Novel Phase of Aggregation in the Presence of HS*—In addition to promoting the conversion from the native state into an aggregation-prone, partially folded state, HS has also been found to have a dramatic effect on the self-assembly of the resulting conformational state into aggregates. Our kinetic analysis reveals that this effect does not consist of a simple HS-mediated acceleration of this self-assembly step. Two phases of aggregation are observed in the presence of HS. The first phase is very rapid, occurs on the time scale of a few seconds, and is missing in the absence of HS. It is monitored as an increase of ThT fluorescence (Fig. 4*A*), as an increase of light scattering intensity (Fig. 5*A*), as the appearance of slow-diffusing species with DLS (Fig. 7*B*), as the appearance of oligomers with AFM (Fig. 8*C*), and as an enrichment of β-sheet structure (Fig. 3*C*). This phase is a real aggregation event rather than a HS-induced conformational change occurring within the monomeric TFE-denatured state. This is supported by the observed immediate increase of both the ThT fluorescence and light scattering signal (Figs. 4*A* and 5*A*), by the detection of aggregated species via DLS and AFM (Figs. 7*B* and 8*C*), and by the suppression of the spectroscopic changes associated with such phase when aggregates are removed from the sample at the end of this phase through filtration (Fig. 6*A*). Remarkably, the amplitude of this phase increases linearly with HS concentration (Figs. 4*B* and 5*B*), suggesting that the number of molecules aggregating via this phase increases with HS concentration.

The second phase is slower and occurs on a time scale of ~1 h. This phase can be monitored as a further increase of ThT fluorescence and light scattering (Figs. 4*A* and 5*A*), as the acquisition of extensive β-sheet structure (Fig. 3, *A* and *C*), and as the accumulation of large protofibrils (Figs. 7*B* and 8*D*). This phase appears to be an event occurring in parallel with and independently of the first phase rather than arising from the reorganization or further association of the aggregates formed through the first phase in a sequential mechanism. Several lines of evidence support this conclusion. First, the amplitude and rate of the second phase do not show any dependence on HS concentration (Figs. 4, *C* and *E*, and 5*C*). If the second phase observed in the presence of HS derived sequentially from the first phase, its parameters would be anticipated to change with HS concentration. Second, the observation that the amplitude of the first phase depends on HS concentration, whereas the amplitude of the second phase does not (Figs. 4, *B* and *C*, and 5, *B* and *C*), is not consistent with a sequential mechanism (in this case, the amplitude of the second phase would be expected to increase concomitantly with that of the first phase). Third, and more importantly, the elimination of the aggregates formed through

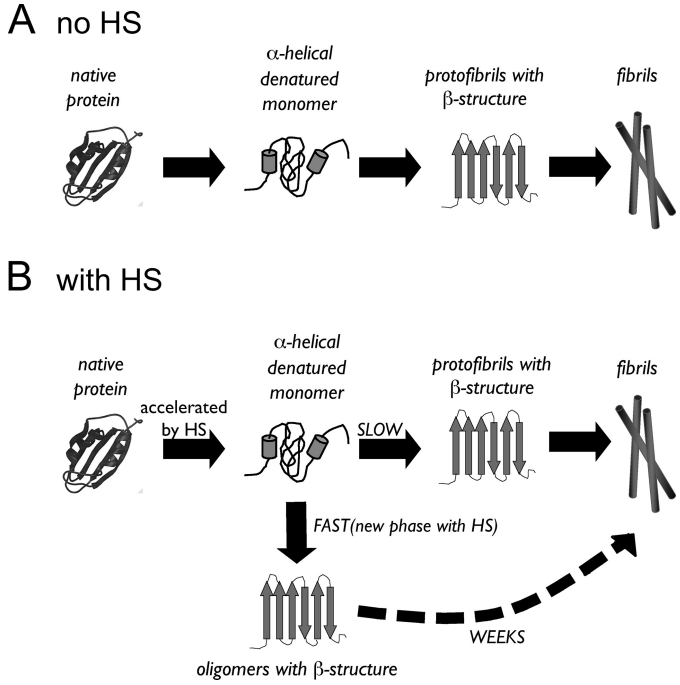


FIGURE 9. **Proposed model for the formation of amyloid-like protofibrils from mAcP in the presence of HS.** *A*, model for amyloid formation from mAcP without HS. Native mAcP converts from its native state to a TFE-denatured state that is enriched in $\alpha$-helical structure and subsequently forms amyloid-like protofibrils enriched with $\beta$-sheet structure. Fibrils will form from such species on the time scale of weeks. *B*, model for amyloid formation from mAcP in the presence of HS. Native mAcP converts from its native state to a TFE-denatured state that is enriched with $\alpha$-helical structure, a step that is accelerated by HS. Subsequently, the protein pool is divided into two fractions, and two processes occur in parallel. A small fraction of protein molecules follows a rapid pathway and is quickly converted into ThT-positive and $\beta$-sheet-containing oligomers, depleting available HS. This represents a new phase that was not observed in the absence of HS. The remaining fraction of the protein pool, which does not interact with HS, follows a normal slow pathway and is converted into amyloid-like protofibrils with ThT-binding and $\beta$-sheet structure showing the same kinetic features as in the absence of HS. Fibrils are likely to form from both species on the time scale of weeks.

the first phase via filtration does not suppress the second phase (Fig. 6*A*), indicating that the two phases occur independently of each other. Fourth, the presence of a large pool of monomeric, TFE-denatured mAcP at the end of the first phase (Fig. 7*B*) excludes further the possibility that all mAcP molecules aggregate via the fast phase and that the second phase represents only a structural reorganization or further assembly of the initially formed aggregates.

*A Model Describing Aggregation of mAcP in the Presence of HS*—A model that accounts for all of the experimental data is depicted in Fig. 9. Native mAcP first converts into an aggregation-competent partially folded state, a process that is accelerated by HS, as discussed above. The resulting conformational state of mAcP can take two pathways in the presence of HS. A fraction of the mAcP molecules is affected by HS and aggregates via a very rapid pathway to form ThT-positive and $\beta$-sheet-containing oligomers. Only a fraction of mAcP molecules can take this pathway, because HS concentration is a limiting factor. Indeed, the concentration range of HS used here (0.5–10 $\mu$g/ml) corresponds to an effective concentration of its sulfate moieties from $\sim$2 $\mu$M (0.5 $\mu$g/ml HS) to $\sim$45 $\mu$M (10 $\mu$g/ml HS), much lower than the effective concentration of positive charges in mAcP, which is 546 $\mu$M under the conditions used here. Hence, even with the highest HS concentration employed in our tests, the molarities of mAcP and of its positive charges exceed those of HS and its sulfate moieties, respectively. Consequently, only a small fraction of mAcP interacts with HS, aggregating rapidly and depleting its availability.

The finding that ThT fluorescence increases remarkably following the first rapid phase indicates that the fraction of mAcP molecules aggregating via the first phase, albeit small, reaches a notable structural order. Moreover, the observation that HS needs to be present at the start of the aggregation process to promote this rapid aggregation phase (Fig. 6*B*) indicates that the interaction between mAcP and HS occurs early in the process, before the protein is denatured to form the aggregation-prone state. Thus, the first rapid phase of aggregation involves the aggregation process of a fraction of initially native protein molecules that bind to HS, unfold after binding, and immediately aggregate on the HS surface. The appearance of a new rapid phase of aggregation does not, however, simply result from the HS-mediated acceleration of the initial conformational change occurring on monomeric mAcP. Indeed, the first aggregation phase is severalfold more rapid than the second slow phase and cannot result from the 2-fold HS-mediated acceleration of the initial conformational change.

The majority of mAcP molecules cannot interact with HS and follow a slow aggregation pathway, which occurs in parallel with the rapid step and shares basically the same kinetic characteristics observed in the absence of HS. It is likely that both species formed with and without the assistance of HS will eventually form fibrils on the time scale of weeks (35).

This model explains why the amplitude of the first phase is linearly related to HS concentration and why the amplitude of the slow phase undergoes no significant change or at most just a small decrease (as observed in Fig. 4*C*). The model is also consistent with the finding that the first far-UV CD spectrum recorded in the presence of HS, after the first phase and before the second phase, is a mixed $\alpha/\beta$ spectrum, with $\alpha$-helical structure dominating. Indeed, at this stage, the aggregates with $\beta$-structure formed rapidly upon interaction with HS coexist with the $\alpha$-helical enriched TFE-denatured state that has not yet undergone aggregation.

*HS-assisted Formation of Oligomers*—It is important to notice that the HS-assisted aggregation occurring through the fast phase does not lead to amyloid-like protofibrils or fibrils but to oligomers, as shown by AFM (Fig. 8*C*). These oligomers are small in size (the apparent diameter of $\sim$80 nm determined from DLS arises from clusters of such aggregates, given the tendency of this technique to visualize only the biggest aggregates in a sample). The oligomers bind ThT and increase its fluorescence, display extensive $\beta$-sheet structure, and thus seem to share structural features with real amyloid. Species of this type have been observed to form in the absence of GAGs by many other systems, and for some protein deposition diseases are proposed to be the pathogenic species (1). The enhanced formation of such species by HS can thus be an important phenomenon not just in the overall process of amyloid fibril formation but also in pathogenesis.

*Implications for a Correct Interpretation of the HS-induced Amyloidogenesis*—The data presented here have shown that two phases of aggregation appear in the presence of HS and that only the first step, dramatically accelerated with respect to that observed in the absence of HS, can be attributed to an HS-induced aggregation. The HS-mediated appearance of a new phase in the aggregation process is not a peculiar and exceptional trait of the protein and experimental conditions used here. It is commonly observed in the time course of aggregation of other systems, when HS or its highly sulfated analogue heparin is present (14, 18, 22, 48, 49), although in some other cases it is not (16, 17).

The assignment of the observed phases to well defined aggregation events is necessary to quantify the impact of HS on amyloid formation. We can better stress this concept through an example. If the rate and final ThT fluorescence were the only parameters considered in our results, one would conclude that (i) HS does not affect the rate of mAcP aggregation, and (ii) HS only brings about more order within the aggregates. This is clearly a misinterpretation of the data, since the analysis shows, by contrast, that HS causes a dramatic acceleration of mAcP aggregation and induces considerable order in the molecules aggregating via a direct interaction with HS. The ability of HS to split the aggregation process into two pathways occurring independently of each other is also a systematically neglected issue.

*Conclusions*—Overall, the data indicate that HS can have a dramatic effect on amyloid formation by mAcP. It can both destabilize the initial folded state, accelerating its transition to the aggregation-prone state, and cause a severalfold acceleration upon the subsequent self-assembly of partially unfolded monomers into ThT-positive and $\beta$-sheet-containing oligomers, with the latter effect appearing to be larger than previously thought. In the lamina densa of the basal membrane, where HS is abundant as side chains of large proteoglycans, the kinetics and pathway influenced by HS can dominate over those observed in their absence and lead to oligomeric species that are often thought to be the real pathogenic species in amyloid-associated diseases. This not only leads to accelerated and enhanced amyloid-fibril formation and deposition but also determines a pathway distinct from that commonly observed *in vitro* in the absence of HS and other GAGs.

*Acknowledgment—We thank Francesco Bemporad for technical assistance.*

## REFERENCES


1. Chiti, F., and Dobson, C. M. (2006) *Annu. Rev. Biochem.* **75,** 333–366
2. Stefani, M., and Dobson, C. M. (2003) *J. Mol. Med.* **81,** 678–699
3. Alexandrescu, A. T. (2005) *Protein Sci.* **14,** 1–12
4. Ancsin, J. B. (2003) *Amyloid-J. Protein Fold. Disord.* **10,** 67–79
5. Bosman, F. T., and Stamenkovic, I. (2003) *J. Pathol.* **200,** 423–428
6. Snow, A. D., Kisilevsky, R., Stephens, C., and Anastassiades, T. (1987) *Lab. Invest.* **56,** 665–675
7. Young, I. D., Willmer, J. P., and Kisilevsky, R. (1989) *Acta Neuropathol.* **78,** 202–209
8. Magnus, J. H., Stenstad, T., Kolset, S. O., and Husby, G. (1991) *Scand. J. Immunol.* **34,** 63–69
9. van Duinen, S. G., Maat-Schieman, M. L., Bruijn, J. A., Haan, J., and Roos, R. A. (1995) *Lab. Invest.* **73,** 183–189
10. Snow, A. D., Mar, H., Nochlin, D., Kimata, K., Kato, M., Suzuki, S., Hassell, J., and Wight, T. N. (1988) *Am. J. Pathol.* **133,** 456–463
11. Young, I. D., Ailles, L., Narindrasorasak, S., Tan, R., and Kisilevsky, R. (1992) *Arch. Pathol. Lab. Med.* **116,** 951–954
12. Snow, A. D., Wight, T. N., Nochlin, D., Koike, Y., Kimata, K., DeArmond, S. J., and Prusiner, S. B. (1990) *Lab. Invest.* **63,** 601–611
13. McLaurin, J., Franklin, T., Zhang, X., Deng, J., and Fraser, P. E. (1999) *Eur. J. Biochem.* **266,** 1101–1110
14. Cotman, S. L., Halfter, W., and Cole, G. J. (2000) *Mol. Cell Neurosci.* **15,** 183–198
15. Castillo, G. M., Cummings, J. A., Yang, W., Judge, M. E., Sheardown, M. J., Rimvall, K., Hansen, J. B., and Snow, A. D. (1998) *Diabetes* **47,** 612–620
16. Cohlberg, J. A., Li, J., Uversky, V. N., and Fink, A. L. (2002) *Biochemistry* **41,** 1502–1511
17. Suk, J. Y., Zhang, F., Balch, W. E., Linhardt, R. J., and Kelly, J. W. (2006) *Biochemistry* **45,** 2234–2242
18. Yamaguchi, I., Suda, H., Tsuzuike, N., Seto, K., Seki, M., Yamaguchi, Y., Hasegawa, K., Takahashi, N., Yamamoto, S., Gejyo, F., and Naiki, H. (2003) *Kidney Int.* **64,** 1080–1088
19. Goedert, M., Jakes, R., Spillantini, M. G., Hasegawa, M., Smith, M. J., and Crowther, R. A. (1996) *Nature* **383,** 550–553
20. de Beer, M. C., de Beer, F. C., McCubbin, W. D., Kay, C. M., and Kindy, M. S. (1993) *J. Biol. Chem.* **268,** 20606–20612
21. McCubbin, W. D., Kay, C. M., Narindrasorasak, S., and Kisilevsky, R. (1988) *Biochem. J.* **256,** 775–783
22. Wong, C., Xiong, L. W., Horiuchi, M., Raymond, L., Wehrly, K., Chesebro, B., and Caughey, B. (2001) *EMBO J.* **20,** 377–386
23. Pastore, A., Saudek, V., Ramponi, G., and Williams, R. J. (1992) *J. Mol. Biol.* **224,** 427–440
24. Stefani, M., Taddei, N., and Ramponi, G. (1997) *Cell Mol. Life Sci.* **53,** 141–151
25. Chiti, F., Calamai, M., Taddei, N., Stefani, M., Ramponi, G., and Dobson, C. M. (2002) *Proc. Natl. Acad. Sci. U.S.A.* **99,** Suppl. 4, 16419–16426
26. Chiti, F., Taddei, N., Bucciantini, M., White, P., Ramponi, G., and Dobson, C. M. (2000) *EMBO J.* **19,** 1441–1449
27. Calamai, M., Chiti, F., and Dobson, C. M. (2005) *Biophys. J.* **89,** 4201–4210
28. Calamai, M., Taddei, N., Stefani, M., Ramponi, G., and Chiti, F. (2003) *Biochemistry* **42,** 15078–15083
29. Chiti, F., Taddei, N., Stefani, M., Dobson, C. M., and Ramponi, G. (2001) *Protein Sci.* **10,** 879–886
30. Taddei, N., Capanni, C., Chiti, F., Stefani, M., Dobson, C. M., and Ramponi, G. (2001) *J. Biol. Chem.* **276,** 37149–37154
31. Chiti, F., Stefani, M., Taddei, N., Ramponi, G., and Dobson, C. M. (2003) *Nature* **424,** 805–808
32. Monti, M., Garolla di Bard, B. L., Calloni, G., Chiti, F., Amoresano, A., Ramponi, G., and Pucci, P. (2004) *J. Mol. Biol.* **336,** 253–262
33. Bemporad, F., Taddei, N., Stefani, M., and Chiti, F. (2006) *Protein Sci.* **15,** 862–870
34. Calamai, M., Kumita, J. R., Mifsud, J., Parrini, C., Ramazzotti, M., Ramponi, G., Taddei, N., Chiti, F., and Dobson, C. M. (2006) *Biochemistry* **45,** 12806–12815
35. Chiti, F., Webster, P., Taddei, N., Clark, A., Stefani, M., Ramponi, G., and Dobson, C. M. (1999) *Proc. Natl. Acad. Sci. U.S.A.* **96,** 3590–3594
36. Modesti, A., Taddei, N., Bucciantini, M., Stefani, M., Colombini, B., Raugei, G., and Ramponi, G. (1995) *Protein Expr. Purif.* **6,** 799–805
37. van Nuland, N. A., Chiti, F., Taddei, N., Raugei, G., Ramponi, G., and Dobson, C. M. (1998) *J. Mol. Biol.* **283,** 883–891
38. Chiti, F., Taddei, N., Baroni, F., Capanni, C., Stefani, M., Ramponi, G., and Dobson, C. M. (2002) *Nat. Struct. Biol.* **9,** 137–143
39. Chiti, F., Taddei, N., Webster, P., Hamada, D., Fiaschi, T., Ramponi, G., and Dobson, C. M. (1999) *Nat. Struct. Biol.* **6,** 380–387
40. Booth, D. R., Sunde, M., Bellotti, V., Robinson, C. V., Hutchinson, W. L., Fraser, P. E., Hawkins, P. N., Dobson, C. M., Radford, S. E., Blake, C. C., and Pepys, M. B. (1997) *Nature* **385,** 787–793
41. McParland, V. J., Kad, N. M., Kalverda, A. P., Brown, A., Kirwin-Jones, P.,

Hunter, M. G., Sunde, M., and Radford, S. E. (2000) *Biochemistry* **39,** 8735–8746
42. Kim, Y. S., Randolph, T. W., Stevens, F. J., and Carpenter, J. F. (2002) *J. Biol. Chem.* **277,** 27240–27246
43. Lai, Z., Colón, W., and Kelly, J. W. (1996) *Biochemistry* **35,** 6470–6482
44. Raffen, R., Dieckman, L. J., Szpunar, M., Wunschl, C., Pokkuluri, P. R., Dave, P., Wilkins Stevens, P., Cai, X., Schiffer, M., and Stevens, F. J. (1999) *Protein Sci.* **8,** 509–517
45. Sekijima, Y., Wiseman, R. L., Matteson, J., Hammarström, P., Miller, S. R., Sawkar, A. R., Balch, W. E., and Kelly, J. W. (2005) *Cell* **121,** 73–85
46. Smith, D. P., Jones, S., Serpell, L. C., Sunde, M., and Radford, S. E. (2003) *J. Mol. Biol.* **330,** 943–954
47. Chiti, F., and Dobson, C. M. (2009) *Nat. Chem. Biol.* **5,** 15–22
48. Takase, K. (1998) *FEBS Lett.* **441,** 271–274
49. Meng, F., Abedini, A., Song, B., and Raleigh, D. P. (2007) *Biochemistry* **46,** 12091–12099